Nanoscale Advances

ROYAL SOCIETY OF CHEMISTRY

PAPER

View Article Online
View Journal | View Issue

Open Access Article. Published on 15 November 2023. Downloaded on 7/29/2025 9:28:29 PM.
This article is licensed under a Creative Commons Attribution-NonCommercial 3.0 Unported Licence.

Check for updates

Cite this: *Nanoscale Adv.*, 2023, **5**, 6967

A dissipative and entropy-optimized MHD nanomaterial mixed convective flow for engineering applications

Faqir Shah,[a] Tasawar Hayat,[b] Asad Ullah,[a] Sohail A. Khan *[b] and Shaher Momani[c]

Received 17th July 2023
Accepted 31st October 2023

DOI: 10.1039/d3na00538k

rsc.li/nanoscale-advances

Background and objective: Nanomaterials play significant roles in numerous industrial and engineering applications, like nuclear plants, paper production, thermal power plants, glass fibres, manufacturing of medicines, medical instruments, micro-electronics and polymer sheet extrusion. In view of such important applications, in this study, we discuss the magnetohydrodynamic flow of a nanofluid over an inclined surface by employing the Darcy–Forchheimer model. The Buongiorno model is applied to understand the various important aspects of the nanofluid. Radiation, magnetic field, dissipation and entropy generation in a chemically reactive flow are also discussed. *Methodology*: The governing nonlinear expressions were transformed into a dimensionless system through adequate transformations. The obtained non-dimensional systems were computed by the NDSolve approach. *Results*: Physical illustrations for the flow, temperature, concentration and entropy rate *via* emerging variables were examined. Here an enhancement in velocity was seen for the mixed convection variable, while opposite impacts on flow and temperature were noticed through the Hartman number. A higher Eckert number was obtained with a rise in temperature, while a decrease in concentration was noticed for the thermophoresis variable. An augmentation in the entropy rate was detected for radiation, while the thermal transport rate was boosted by thermophoresis.

1 Introduction

Nanofluids are a mixture of nano-sized (1–100 nm) solid particles (metals, carbides, oxides and carbon nanotubes) and conventional fluids (water, lubricant oil, ethylene and propylene glycol). Nanofluids play a vital role in the heat-transfer processes of conventional liquids. Nanomaterials play significant roles in numerous industrial and engineering applications, like nuclear plants, paper production, thermal power plants, glass fibre, manufacturing of medicines, medical instruments, microelectronics and polymer sheet extrusion. The thermal conduction processes of conventional materials can be improved by the addition of nano-sized particles. Various industrial processes face a low-heat transportation problem caused by the utilization of conventional fluids. This issue is often tackled by using nanofluids and hybrid nanomaterials. The enhancement of the thermal conductivity of conventional materials through the addition of nano-sized metallic particles was first reported by Choi.[1] Buongiorno[2] later gave a mathematical model and discussed seven slip mechanisms for the enhancement of the thermal characteristics of fluids, with Brownian motion and thermophoresis as the most important factors. Waini *et al.*[3] reported on the magnetohydrodynamic radiative flow of a Reiner–Philippoff nanoliquid subjected to a random motion and thermophoresis. Heat transfer in the electrically conductive flow of a nanoliquid with thermophoresis and random motion was discussed by Kalpana *et al.*[4] The hydromagnetic convective flow of an Eyring–Powell nanomaterial considering multiple diffusions was analysed by Patil and Kulkarni.[5] Random and thermophoresis diffusions for a Casson nanoliquid flow considering a gyrotactic microorganism was studied by Upreti *et al.*[6] Ohmic heating in the magnetized convective flow of a Reiner–Rivlin nanoliquid considering the entropy rate was explored by Khan *et al.*[7] Cattaneo–Christov fluxes for the bioconvective flow of a Maxwell nanomaterial subjected to the Arrhenius activation energy were examined by Bagh *et al.*[8] Some further related studies on nanomaterials are listed in ref. 9–20.

Measurement of the wastage energy in any thermodynamical system refers to the entropy. Entropy generation is an important thermodynamical approach that is used to analyse the thermal performance of systems in industrial and engineering fields. Entropy is produced due to heat transfer, molecule collision, thermal radiation, Joule heating, diffusion, fluid friction, and spinning motion, *etc.* In any thermodynamical system, a significant part of the thermal energy is wasted, meaning it is not fully utilized for useful work. Therefore, several researchers have paid attention to this important issue. Bejan[21,22] was the first to

[a]Department of Mathematical Sciences, Karakoram International University Gilgit, Gilgit 15100, Pakistan
[b]Department of Mathematics, Quaid-I-Azam University, Islamabad 44000, Pakistan. E-mail: sohailahmadkhan93@gmail.com
[c]Nonlinear Dynamics Research (NDRC), Ajman University, Ajman, United Arab Emirates

© 2023 The Author(s). Published by the Royal Society of Chemistry

Open Access Article. Published on 15 November 2023. Downloaded on 7/29/2025 9:28:29 PM.
This article is licensed under a Creative Commons Attribution-NonCommercial 3.0 Unported Licence.

introduce entropy minimization in convective flow. Entropy in the squeezing flow of a CNT nanoliquid was examined by Dawar *et al.*[23] Hayat *et al.*[24] investigated an unsteady nanoliquid flow considering Sort and Dufour characteristics. A few important studies concerning the entropy rate are mentioned in ref. 25–32.

Our prime objective here was to analyse the magnetohydrodynamic convective flow of a nanoliquid by an inclined surface. The Darcy–Forchheimer relation was considered and is discussed in this context. Radiation, magnetic field, and dissipation were considered in relation to energy. Brownian motion and thermophoresis diffusion were accounted for. The entropy rate for a chemically reactive flow was studied. Nonlinear partial differential equations were reduced to non-dimensional systems through suitable transformation. The ND-solve technique was implemented for the computations. Graphical discussions were used to consider the flow, Nusselt number, entropy rate, drag force, concentration, and temperature *via* sundry variables.

2 Statement

The hydromagnetic mixed convective flow of a nanoliquid over an inclined surface is studied. The Darcy–Forchheimer relation was considered here. Random and thermophoresis diffusions were accounted. Dissipation, magnetic field Joule heating, first-order reaction, and radiation were also taken into account. Entropy optimization for the chemically reactive flow was elaborated. Flow tests in the presence of a constant magnetic field were conducted. A sketch of the problem is presented in Fig. 1.[33]

Here, the governing expressions satisfy:[24–28]

$$\frac{\partial u}{\partial x}+\frac{\partial v}{\partial y}=0, \tag{1}$$

$$\left.\begin{array}{l} u\dfrac{\partial u}{\partial x}+v\dfrac{\partial u}{\partial y}=\nu_{\mathrm{f}}\dfrac{\partial^2 u}{\partial y^2}+g\left[(1-C_\infty)\rho_{f_\infty}\beta(T-T_\infty)-(C-C_\infty)(\rho_{\mathrm{p}}-\rho_{f_\infty})\right]\cos\Omega \\ -\dfrac{\sigma_{\mathrm{f}}{B_0}^2}{\rho_{\mathrm{f}}}u-\dfrac{\mu_{\mathrm{f}}}{(\rho_{\mathrm{f}})k_{\mathrm{p}}}-Fu^2 \end{array}\right\}, \tag{2}$$

$$\left.\begin{array}{l} u\dfrac{\partial T}{\partial x}+v\dfrac{\partial T}{\partial y}=\alpha_{\mathrm{f}}\dfrac{\partial^2 T}{\partial y^2}+\dfrac{16\sigma^* T_\infty}{3k^*(\rho c_{\mathrm{p}})_{\mathrm{f}}}\dfrac{\partial^2 T}{\partial y^2}+\tau\left(D_{\mathrm{B}}\dfrac{\partial C}{\partial y}\dfrac{\partial T}{\partial y}+\dfrac{D_{\mathrm{T}}}{T_\infty}\left(\dfrac{\partial T}{\partial y}\right)^2\right) \\ +\dfrac{\mu_{\mathrm{f}}}{(\rho c_{\mathrm{p}})_{\mathrm{f}}}\left(\dfrac{\partial u}{\partial y}\right)^2+\dfrac{\sigma_{\mathrm{f}}{B_0}^2}{(\rho c_{\mathrm{p}})_{\mathrm{f}}}u^2 \end{array}\right\}, \tag{3}$$

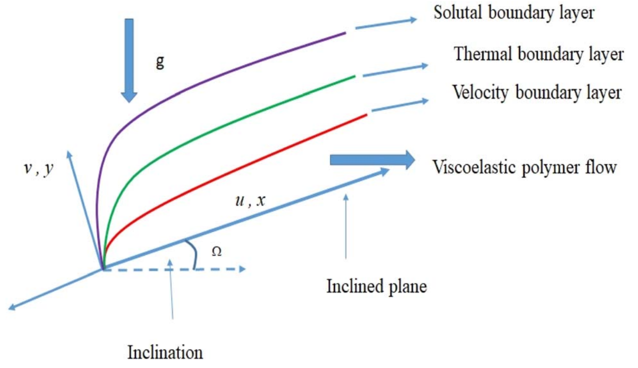

Fig. 1 Flow sketch.

$$u\frac{\partial C}{\partial x}+v\frac{\partial C}{\partial y}=D_{\mathrm{B}}\frac{\partial^2 C}{\partial y^2}+\left(\frac{D_{\mathrm{T}}}{T_\infty}\right)\frac{\partial^2 T}{\partial y^2}-k_{\mathrm{r}}(C-C_\infty), \tag{4}$$

with

$$\left.\begin{array}{c} u=0,\;\; v=0,\;\; T=T_{\mathrm{w}},\;\; D_{\mathrm{B}}\dfrac{\partial C}{\partial y}+\left(\dfrac{D_{\mathrm{T}}}{T_\infty}\right)\dfrac{\partial T}{\partial y}=0\;\text{ at }\; y=0 \\ u=u_\infty,\;\; T\to T_\infty,\;\; C\to C_\infty\;\text{ as }\; y\to\infty. \end{array}\right\}. \tag{5}$$

Letting:[34,35]

$$\left.\begin{array}{l} \zeta=\dfrac{x}{L},\;\; \eta=\dfrac{y}{x}\sqrt{\mathrm{Re}_x},\;\; \psi=\nu\sqrt{\mathrm{Re}_x}f(\zeta,\eta),\;\; \mathrm{Re}_x=\dfrac{u_\infty x}{\nu} \\ \theta(\zeta,\eta)=\dfrac{T-T_\infty}{T_{\mathrm{w}}-T_\infty},\;\; \phi(\zeta,\eta)=\dfrac{C-C_\infty}{C_{\mathrm{w}}-C_\infty},\;\; u=\dfrac{\partial\psi}{\partial y},\;\; v=-\dfrac{\partial\psi}{\partial x} \end{array}\right\}, \tag{6}$$

we get

$$\left.\begin{array}{l} \dfrac{\partial^3 f}{\partial\eta^3}+\dfrac{1}{2}f\dfrac{\partial^2 f}{\partial\eta^2}-\dfrac{\mathrm{Ha}}{\mathrm{Re}}\zeta\dfrac{\partial f}{\partial\eta}+\mathrm{Ri}\zeta(\theta-\mathrm{Nr}\phi)\cos\Omega-\lambda\zeta\dfrac{\partial f}{\partial\eta}-\mathrm{Fr}\zeta\left(\dfrac{\partial f}{\partial\eta}\right)^2 \\ =\zeta\left(\dfrac{\partial f}{\partial\zeta}\dfrac{\partial f}{\partial\eta}-\dfrac{\partial f}{\partial\zeta}\dfrac{\partial^2 f}{\partial\eta^2}\right), \end{array}\right\}, \tag{7}$$

 © 2023 The Author(s). Published by the Royal Society of Chemistry

Open Access Article. Published on 15 November 2023. Downloaded on 7/29/2025 9:28:29 PM.
This article is licensed under a Creative Commons Attribution-NonCommercial 3.0 Unported Licence.

$$\left.\begin{aligned}&\frac{1}{\Pr}\frac{\partial^2\theta}{\partial\eta^2}+\mathrm{Nb}\frac{\partial\varphi}{\partial\eta}\frac{\partial\theta}{\partial\eta}+\mathrm{Nt}\left(\frac{\partial\theta}{\partial\eta}\right)^2+\left(\frac{\mathrm{Ha}}{\mathrm{Re}}\right)\mathrm{Ec}\zeta\left(\frac{\partial f}{\partial\eta}\right)^2+\frac{\mathrm{Rd}}{\Pr}\frac{\partial^2\theta}{\partial\eta^2}\\&+\mathrm{Ec}\left(\frac{\partial^2 f}{\partial\eta^2}\right)^2+\frac{1}{2}f\frac{\partial\theta}{\partial\eta}=\zeta\left(\frac{\partial\theta}{\partial\zeta}-\frac{\partial f}{\partial\zeta}\frac{\partial\theta}{\partial\eta}\right)\end{aligned}\right\},\tag{8}$$

$$\left.\begin{aligned}&\frac{\partial f(\zeta,0)}{\partial\eta}=0,\quad f(\zeta,0)=-\zeta\frac{\partial f(\zeta,0)}{\partial\zeta},\quad\theta(0)=1,\quad\mathrm{Nb}\frac{\partial\varphi(\zeta,0)}{\partial\eta}+\mathrm{Nt}\frac{\partial\theta(\zeta,0)}{\partial\eta}=0,\quad\text{as }\eta=0\\&\frac{\partial f(\zeta,\infty)}{\partial\eta}=1,\quad\theta(\zeta,\infty)=0,\quad\phi(\zeta,\infty)=0,\quad\text{as }\eta\to\infty\end{aligned}\right\}.\tag{9}$$

subject to conditions

$$\left.\begin{aligned}&\frac{\partial f(\zeta,0)}{\partial\eta}=0,\quad f(\zeta,0)=-\zeta\frac{\partial f(\zeta,0)}{\partial\zeta},\quad\theta(0)=1,\quad\mathrm{Nb}\frac{\partial\varphi(\zeta,0)}{\partial\eta}+\mathrm{Nt}\frac{\partial\theta(\zeta,0)}{\partial\eta}=0,\quad\text{as }\eta=0\\&\frac{\partial f(\zeta,\infty)}{\partial\eta}=1,\quad\theta(\zeta,\infty)=0,\quad\phi(\zeta,\infty)=0,\quad\text{as }\eta\to\infty\end{aligned}\right\}.\tag{10}$$

Here the non-dimensional parameters are $\mathrm{Ha}=\left(\frac{\sigma_f {B_0}^2L^2}{\mu}\right)$, $\mathrm{Re}=\left(\frac{u_\infty L}{\nu}\right)$, $\mathrm{Nt}=\left(\frac{\rho c_p D_T(T_w-T_\infty)}{\nu(\rho c)_f T_\infty}\right)$, $\Pr=\left(\frac{\mu C_p}{k}\right)$, $\mathrm{Rd}=\left(\frac{16\sigma^*}{3k^*k}T_\infty^3\right)$, $\mathrm{Ec}=\left(\frac{u_\infty^2}{C_p(T_w-T_\infty)}\right)$, $\mathrm{Sc}=\left(\frac{\nu}{D_B}\right)$, $\mathrm{Nb}=\left(\frac{\rho c_p D_B(C_w-C_\infty)}{\nu(\rho c)_f}\right)$, $\mathrm{Br}=\left(\frac{\mu u_\infty^2}{k(T_w-T_\infty)}\right)$, $k_1=\left(\frac{K_r L}{u_\infty}\right)$, $N_r=\left(\frac{(\rho_p-\rho_{f_\infty})(C_w-C_\infty)}{\beta\rho_{f_\infty}(1-C_\infty)(T_w-T_\infty)}\right)$, $\mathrm{Fr}=\left(\frac{C_b L}{\sqrt{k_p}}\right)$, $\lambda=\left(\frac{\nu L}{u_\infty k_p}\right)$, $\mathrm{Gr}=\left(\frac{g\beta(1-C_\infty)(T_w-T_\infty)}{\nu^2}L^3\right)$ and $\mathrm{Ri}\left(\frac{\mathrm{Gr}}{\mathrm{Re}^2}\right)$.

2.1 Solution

First-order truncation:

In 1st order truncation we assume the derivatives w.r.t. ζ are zero. *i.e.* $\frac{\partial(\cdot)}{\partial\zeta}=0$ then eqn (7)–(10) become,

$$f'''+\frac{1}{2}ff''-\frac{\mathrm{Ha}}{\mathrm{Re}}\zeta f'+\mathrm{Ri}\zeta(\theta-N_r\phi)\cos\Omega-\lambda\zeta f'-\mathrm{Fr}\zeta f'^2=0,\tag{11}$$

$$\frac{1}{\Pr}\theta''+\mathrm{Nb}\phi'\theta'+\mathrm{Nt}\theta'^2+\left(\frac{\mathrm{Ha}}{\mathrm{Re}}\right)\mathrm{Ec}\zeta f'^2+\frac{\mathrm{Rd}}{\Pr}\theta''+\mathrm{Ec}f''^2+\frac{1}{2}f\theta'=0,\tag{12}$$

$$\frac{\phi''}{\mathrm{Sc}}+\frac{\mathrm{Nt}}{\mathrm{ScNb}}\theta''+\frac{1}{2}f\phi'-k_1\zeta\phi=0\tag{13}$$

subject to the conditions

$$\left.\begin{aligned}&f(0)=0,\quad f'(0)=0,\quad\theta(0)=1,\quad\mathrm{Nb}\phi'(0)+\mathrm{Nt}\theta'(0)=0\\&f'(\infty)=1,\quad\theta(\infty)=0,\quad\phi(\infty)=0\end{aligned}\right\}.\tag{14}$$

Second-order truncation:

Here we consider $\frac{\partial f}{\partial\xi}=p$, $\frac{\partial^2 f}{\partial\xi\partial\eta}=\frac{\partial f'}{\partial\xi}=p'$, $\frac{\partial\theta}{\partial\xi}=q$, $\frac{\partial^2\theta}{\partial\xi\partial\eta}=\frac{\partial\theta'}{\partial\xi}=q'$, $\frac{\partial\phi}{\partial\xi}=g$, $\frac{\partial^2\phi}{\partial\xi\partial\eta}=\frac{\partial\phi'}{\partial\xi}=g'$ and denote $\frac{\partial(\cdot)}{\partial\eta}$ by primes. Expressions (7)–(10) become

$$\left.\begin{aligned}&\frac{\partial^3 f}{\partial\eta^3}+\frac{1}{2}f\frac{\partial^2 f}{\partial\eta^2}-\frac{\mathrm{Ha}}{\mathrm{Re}}\zeta\frac{\partial f}{\partial\eta}+\mathrm{Ri}\zeta(\theta-N_r\phi)\cos\Omega-\lambda\zeta\frac{\partial f}{\partial\eta}-\mathrm{Fr}\zeta\left(\frac{\partial f}{\partial\eta}\right)^2\\&=\zeta\left(\frac{\partial p}{\partial\eta}\frac{\partial f}{\partial\eta}-p\frac{\partial^2 f}{\partial\eta^2}\right),\end{aligned}\right\}\tag{15}$$

$$\left.\begin{aligned}&\frac{1}{\Pr}\frac{\partial^2\theta}{\partial\eta^2}+\mathrm{Nb}\frac{\partial\phi}{\partial\eta}\frac{\partial\theta}{\partial\eta}+\mathrm{Nt}\left(\frac{\partial\theta}{\partial\eta}\right)^2+\left(\frac{\mathrm{Ha}}{\mathrm{Re}}\right)\mathrm{Ec}\zeta\left(\frac{\partial f}{\partial\eta}\right)^2+\frac{\mathrm{Rd}}{\Pr}\frac{\partial^2\theta}{\partial\eta^2}\\&+\mathrm{Ec}\left(\frac{\partial^2 f}{\partial\eta^2}\right)^2+\frac{1}{2}f\frac{\partial\theta}{\partial\eta}=\zeta\left(q\frac{\partial f}{\partial\eta}-p\frac{\partial\phi}{\partial\eta}\right)\end{aligned}\right\},\tag{16}$$

$$\frac{1}{\mathrm{Sc}}\frac{\partial^2\phi}{\partial\eta^2}+\frac{\mathrm{Nt}}{\mathrm{ScNb}}\frac{\partial^2\theta}{\partial\eta^2}+\frac{1}{2}f\frac{\partial\phi}{\partial\eta}-k_1\zeta\phi=\zeta\left(g\frac{\partial f}{\partial\eta}-p\frac{\partial\phi}{\partial\eta}\right), \quad (17)$$

$$\left.\begin{array}{c}\frac{\partial f(\zeta,0)}{\partial\eta}=0,\quad f(\zeta,0)=-\zeta p(\zeta,0),\quad \theta(0)=1,\quad \mathrm{Nb}\frac{\partial\phi(\zeta,0)}{\partial\eta}+\mathrm{Nt}\frac{\partial\theta(\zeta,0)}{\partial\eta}=0,\quad \text{as}\quad \eta=0\\ \frac{\partial f(\zeta,\infty)}{\partial\eta}=1,\quad \theta(\zeta,\infty)=0,\quad \phi(\zeta,\infty)=0,\quad \text{as}\quad \eta\to\infty\end{array}\right\}. \quad (18)$$

Differentiating eqn (15)–(18) w.r.t. ζ and neglecting the terms $\frac{\partial p(\xi,\eta)}{\partial\xi}$, $\frac{\partial^2 p(\xi,\eta)}{\partial\eta\partial\xi}$, $\frac{\partial q(\xi,\eta)}{\partial\xi}$, $\frac{\partial^2 q(\xi,\eta)}{\partial\eta\partial\xi}$, $\frac{\partial g(\xi,\eta)}{\partial\xi}$, and $\frac{\partial^2 g(\xi,\eta)}{\partial\eta\partial\xi}$ we get

$$\left.\begin{array}{c}p'''+\frac{3}{2}pf''+\frac{1}{2}fp''+\zeta pp''-p'f'-\zeta p'^2-\frac{\mathrm{Ha}}{\mathrm{Re}}f'-\frac{\mathrm{Ha}}{\mathrm{Re}}\zeta p'+\mathrm{Ri}(\theta-\mathrm{Nr}\phi)\cos\Omega\\ +\mathrm{Ri}\zeta(q-N_{\mathrm{r}}g)\cos\Omega-\lambda f'-\lambda\zeta p'-\mathrm{Fr}f'^2-2\mathrm{Fr}\zeta f'p'=0\end{array}\right\}, \quad (19)$$

$$\left.\begin{array}{c}\frac{1}{\mathrm{Pr}}(1+\mathrm{Rd})q''+\frac{3}{2}p\theta'+\frac{1}{2}fq'+\zeta pq'-qf'-\zeta qp'+\mathrm{Nb}\left(\theta'g'+q'\phi'\right)\\ +2\mathrm{Pr}\ \mathrm{Nt}\theta'q'+\frac{\mathrm{Ha}}{\mathrm{Re}}\mathrm{Ec}f'^2+\frac{2\mathrm{Ha}}{\mathrm{Re}}\mathrm{Ec}\zeta f'p'+2\mathrm{Ec}f''p''=0\end{array}\right\}, \quad (20)$$

$$\frac{1}{\mathrm{Sc}}g''+\frac{3}{2}p\phi'+\frac{1}{2}fg'+\zeta pg'-gf'-\zeta gp'+\frac{1}{\mathrm{Sc}}\frac{\mathrm{Nt}}{\mathrm{Nb}}q''-k_1\phi-k_1\zeta g=0, \quad (21)$$

$$\left.\begin{array}{c}p'(\zeta,0)=0, p(\zeta,0)=0,\ q(\zeta,0)=0, \mathrm{Nb}g'(\zeta,0)+\mathrm{Nt}q'(\zeta,0)=0,\\ p'(\zeta,\infty)=0,\quad q(\zeta,\infty)=0,\quad g(\zeta,\infty)=0\end{array}\right\}. \quad (22)$$

3 Physical quantities

3.1 Coefficient of skin fraction

One may write

$$C_\mathrm{f}=\frac{\tau_\mathrm{w}}{\rho_\mathrm{f}u_\mathrm{w}^2}, \quad (23)$$

with shear stress τ_w given by

$$\tau_\mathrm{w}=\mu_\mathrm{f}\left(\frac{\partial u}{\partial y}\right)\bigg|_{y=0}. \quad (24)$$

We now have

$$\frac{1}{2}\mathrm{Re}_x{}^{1/2}C_\mathrm{f}=-f''(0). \quad (25)$$

3.2 Nusselt number

One may define

$$\mathrm{Nu}=\frac{xq_\mathrm{w}}{k_\mathrm{f}(T_\mathrm{w}-T_\infty)}, \quad (26)$$

in which heat flux q_w obeys

$$q_\mathrm{w}=-\left(k_\mathrm{f}+\frac{16\sigma^*T_\infty^3}{3k^*}\right)\left(\frac{\partial T}{\partial z}\right)\bigg|_{z=0}, \quad (27)$$

Finally, we may have

$$\mathrm{Re}_x{}^{-1/2}\mathrm{Nu}=-(1+\mathrm{Rd})\theta'(0). \quad (28)$$

3.3 Sherwood number

Mathematically

$$\mathrm{Sh}=\frac{xJ_\mathrm{w}}{D_\mathrm{B}(C_\mathrm{w}-C_\infty)}, \quad (29)$$

in which mass flux J_w obeys

$$J_\mathrm{w}=-D_\mathrm{B}\left(\frac{\partial C}{\partial z}\right)\bigg|_{z=0}. \quad (30)$$

Open Access Article. Published on 15 November 2023. Downloaded on 7/29/2025 9:28:29 PM. This article is licensed under a Creative Commons Attribution-NonCommercial 3.0 Unported Licence.

 © 2023 The Author(s). Published by the Royal Society of Chemistry

Open Access Article. Published on 15 November 2023. Downloaded on 7/29/2025 9:28:29 PM.
This article is licensed under a Creative Commons Attribution-NonCommercial 3.0 Unported Licence.

From eqn (21) and (22) we have (31)

$$\mathrm{Re}_x^{-1/2}\mathrm{Sh} = -\phi'(0). \tag{31}$$

In which $\mathrm{Re}_x = \left(\frac{u_w x}{\nu}\right)$ depicts the local Reynolds number.

4 Entropy rate

Mathematically one can write

$$\left.\begin{array}{l} N_G = \frac{k_f}{T_\infty^2}\left(1+\frac{16\sigma^* T_\infty^3}{3k^* k_f}\right)\left(\frac{\partial T}{\partial y}\right)^2 + \frac{\mu_f}{T_\infty}\left(\frac{\partial u}{\partial y}\right)^2 + \frac{\sigma_f B_0{}^2}{T_\infty}u^2 \\ \frac{\mu_f}{k_p T_\infty}u^2 + \frac{RD_B}{T_\infty}\left(\frac{\partial T}{\partial y}\frac{\partial C}{\partial y}\right) + \frac{RD_B}{C_\infty}\left(\frac{\partial C}{\partial y}\right)^2 \end{array}\right\}, \tag{32}$$

In the dimensionless version, we have

$$S_g = \alpha_1(1+\mathrm{Rd})\theta'^2 + \mathrm{Br}f''^2 + \lambda\mathrm{Br}\zeta f'^2 + \frac{\mathrm{Ha}}{\mathrm{Re}}\mathrm{Br}\zeta f'^2 + L_1\theta'\phi' + \frac{\alpha_2}{\alpha_1}L_1\phi'^2. \tag{33}$$

Table 1 Comparative analysis of $\mathrm{Re}_x^{-1/2}\mathrm{Nu}$ with the outcomes reported by Wang[36]

Pr	Wang[36]	Recent outcomes
0.07	0.0656	0.065621
0.20	0.1691	0.169109
0.70	0.4539	0.453901
2.00	0.9114	0.911409
7.00	1.8954	1.895412
20.00	3.3539	3.353925

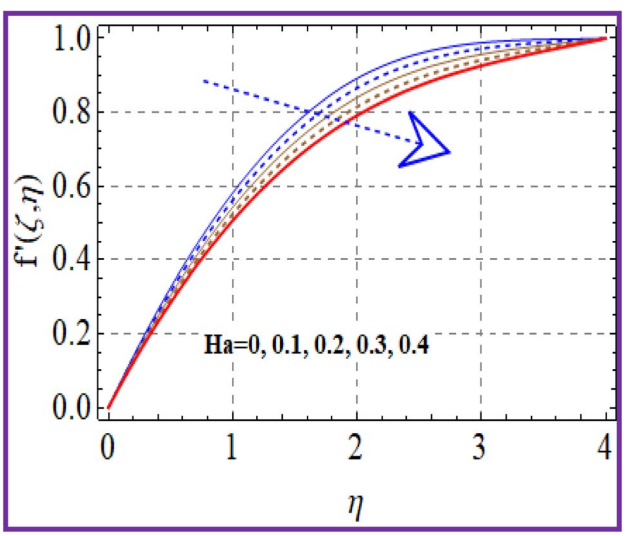

Fig. 2 $f'(\zeta,\eta)$ *via* Ha.

In the above expression, the dimensionless variables are $S_g = \left(\frac{E_G \nu_f T_\infty}{akr^{n-1}(T_w - T_\infty)}\right)$, $\alpha_1 = \left(\frac{T_w - T_\infty}{T_\infty}\right)$, $\alpha_2 = \left(\frac{C_w - C_\infty}{C_\infty}\right)$, and $L_1 = \left(\frac{RD_B(C_w - C_\infty)}{k}\right)$.

5 Analysis

The ND-solve technique was implemented for the solution. The velocity, surface drag force, concentration, Nusselt number, temperature, Bejan number, and entropy rate against the emerging variables were explored. A comparative analysis of the recent outcomes with those by Wang[36] is highlighted in Table 1. Here an outstanding consensus could be noticed.

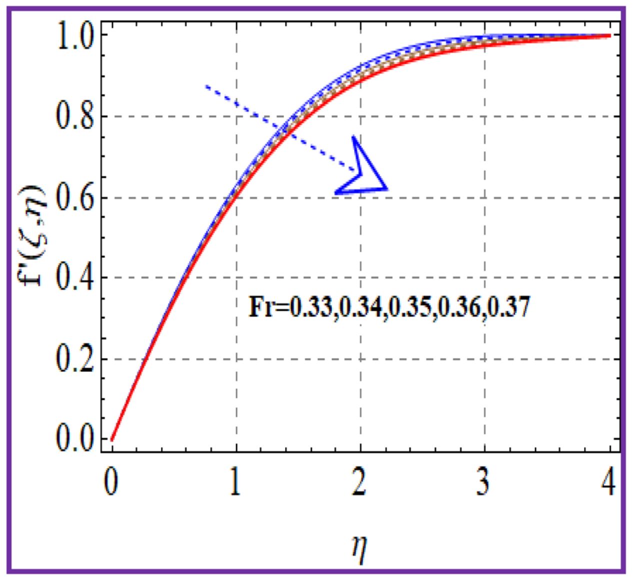

Fig. 3 $f'(\zeta,\eta)$ *via* Fr.

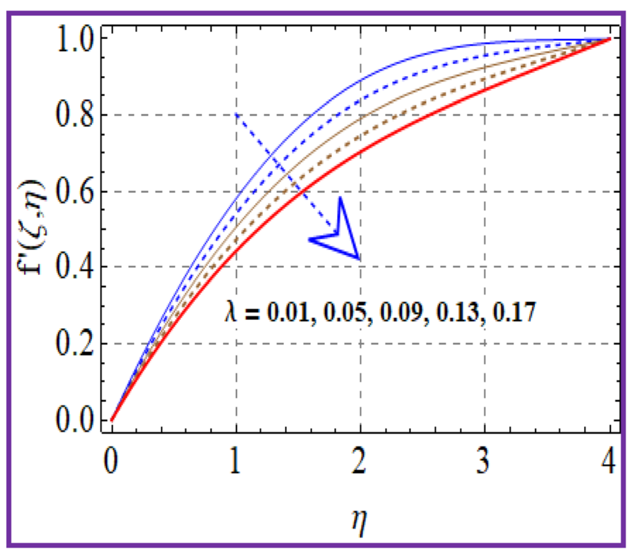

Fig. 4 $f'(\zeta,\eta)$ *via* λ.

Open Access Article. Published on 15 November 2023. Downloaded on 7/29/2025 9:28:29 PM.
This article is licensed under a Creative Commons Attribution-NonCommercial 3.0 Unported Licence.

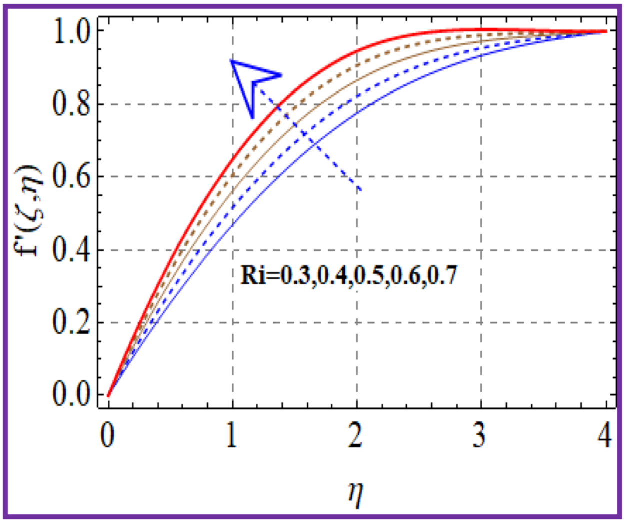

Fig. 5 $f'(\zeta,\eta)$ *via* Ri.

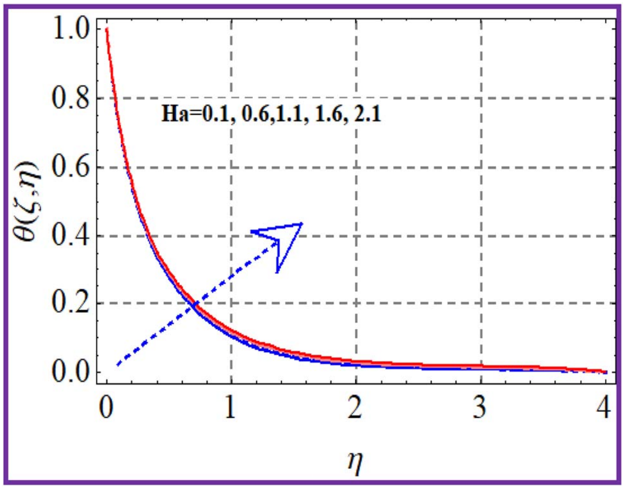

Fig. 6 $\theta(\zeta,\eta)$ *via* Ha.

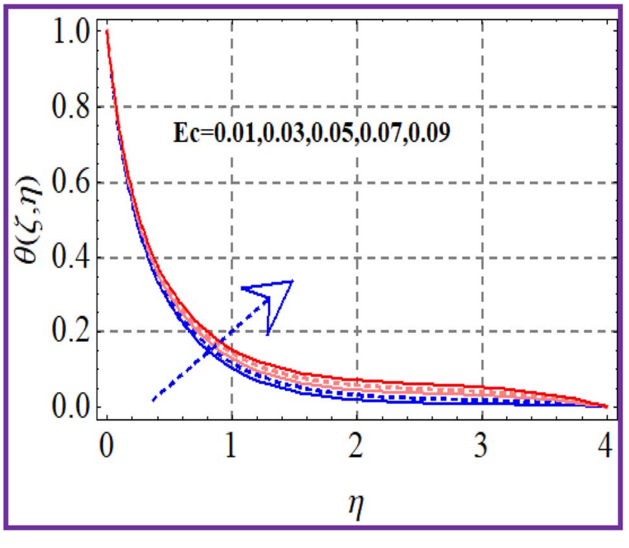

Fig. 7 $\theta(\zeta,\eta)$ *via* Ec.

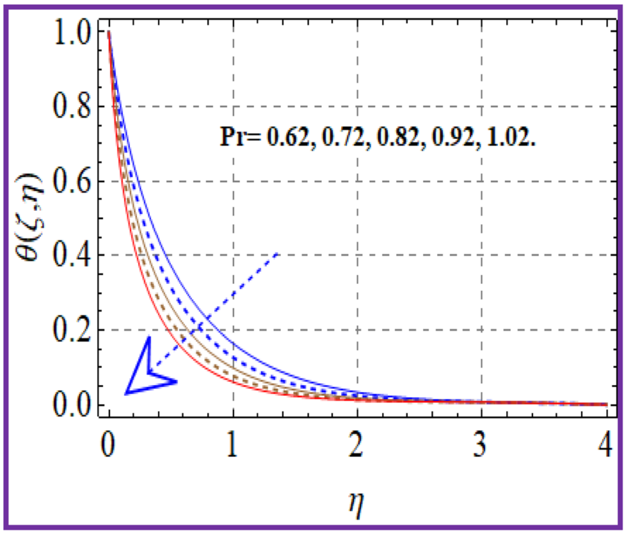

Fig. 8 $\theta(\zeta,\eta)$ *via* Pr.

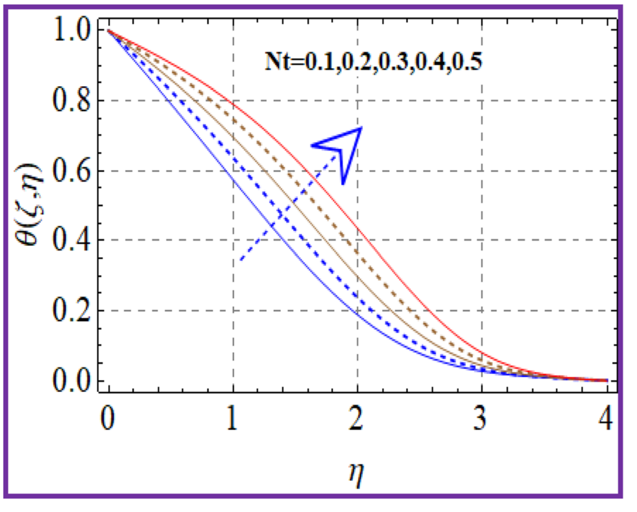

Fig. 9 $\theta(\zeta,\eta)$ *via* Nt.

5.1 Velocity

A plot of the velocity against Hartman number (Ha) is depicted in Fig. 2. A decreasing behavior was noticed for higher Hartman numbers due to the increment in resistive force. The effect of (Fr) on ($f'(\zeta,\eta)$) is portrayed in Fig. 3. A reduction in velocity was noticed for higher Forchheimer (Fr) numbers due to the stronger resistance produced in the fluid flow. The influence of velocity ($f'(\zeta,\eta)$) *via* the porosity parameter (λ) is illustrated in Fig. 4. An increase in the porosity variable corresponded to a more intensive viscous force Therefore the velocity ($f'(\zeta,\eta)$) decayed. A plot of the velocity against the mixed convection variable is illustrated in Fig. 5. An increasing impact on the velocity was noted through utilizing the mixed convection variable.

© 2023 The Author(s). Published by the Royal Society of Chemistry

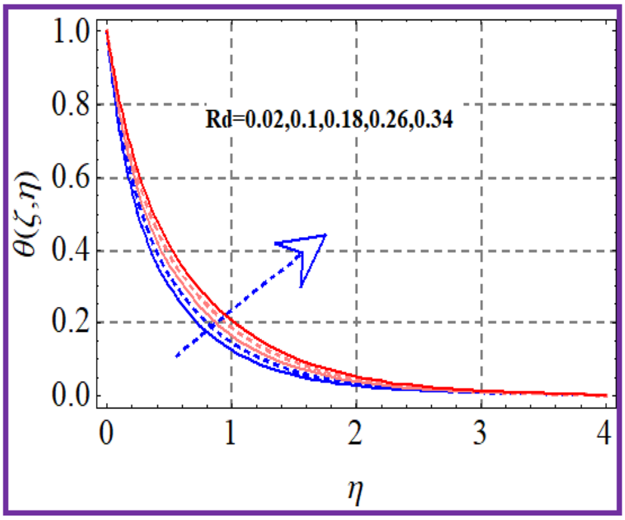

Fig. 10 $\theta(\zeta,\eta)$ *via* Rd.

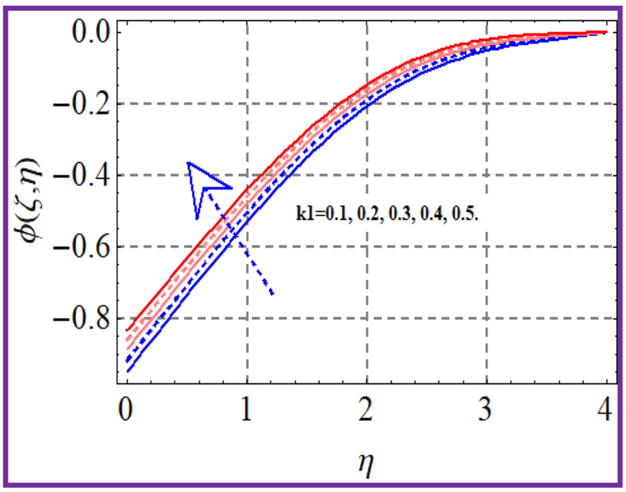

Fig. 11 $\phi(\zeta,\eta)$ *via* k_1.

5.2 Temperature

A plot of temperature *versus* the Hartman number (Ha) in shown in Fig. 6. A larger approximation of the Hartman number increases the Lorentz force, which creates extra heat in the system. Thus the temperature increased. Fig. 7 exhibits the temperature ($\theta(\zeta,\eta)$) performance *versus* the (Ec) Eckert number. The Eckert number increases the kinematic energy of the thermal system, which increases the temperature. A reduction in thermal diffusivity was observed against the Prandtl number, which decreased the temperature (see Fig. 8). The temperature ($\theta(\zeta,\eta)$) behavior with the thermophoresis parameter (Nt) is displayed in Fig. 9. The thermophoresis variable increased the temperature distribution. Fig. 10 shows the impact of radiation (Rd) on the temperature. An enhancement in the thermal field was observed with the radiation variable due to the production of additional energy in the system.

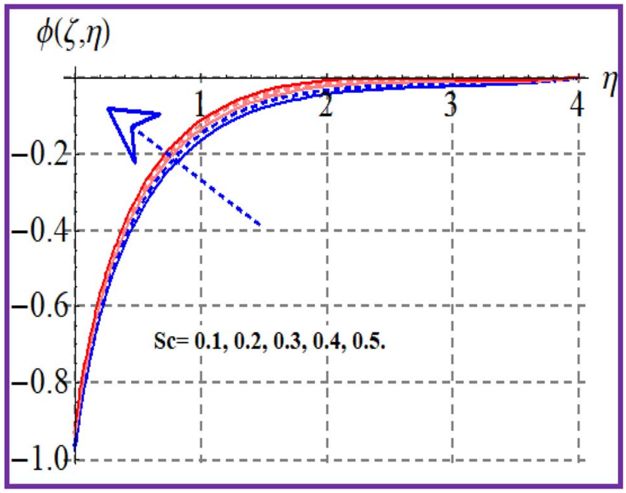

Fig. 12 $\phi(\zeta,\eta)$ *via* Nb.

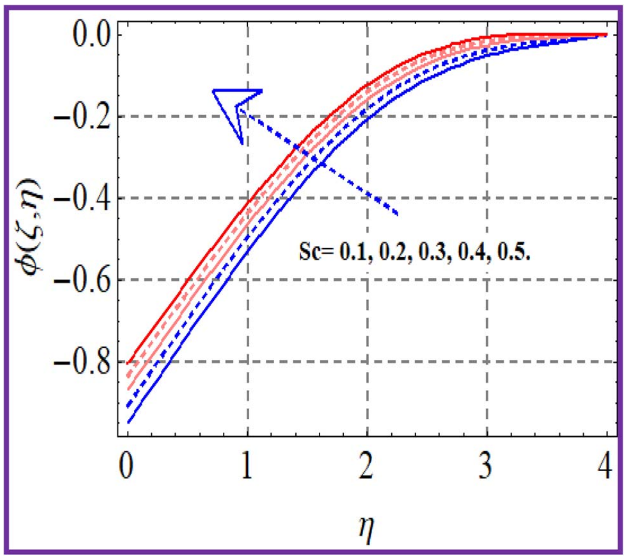

Fig. 13 $\phi(\zeta,\eta)$ *via* Sc.

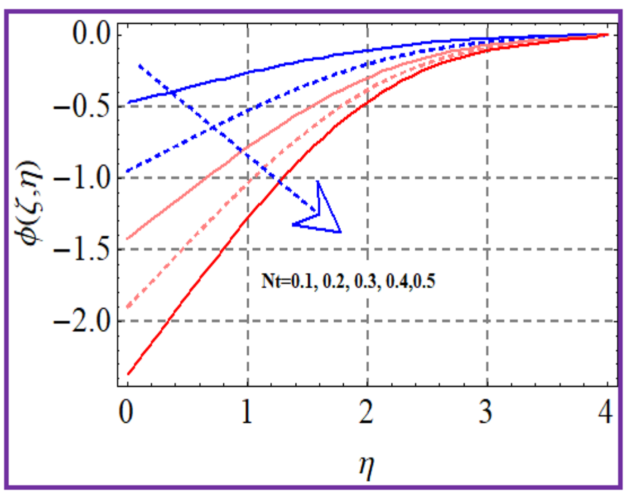

Fig. 14 $\phi(\zeta,\eta)$ *via* Nt.

Open Access Article. Published on 15 November 2023. Downloaded on 7/29/2025 9:28:29 PM.
This article is licensed under a Creative Commons Attribution-NonCommercial 3.0 Unported Licence.

Open Access Article. Published on 15 November 2023. Downloaded on 7/29/2025 9:28:29 PM.
This article is licensed under a Creative Commons Attribution-NonCommercial 3.0 Unported Licence.

5.3 Concentration

The influence of concentration ($\phi(\zeta,\eta)$) with the reaction parameter (k_1) is shown in Fig. 11. An enhancement in concentration was observed with the reaction parameter. The random motion (Nb) impact on the concentration is explored in Fig. 12. Here, the concentration of the nanoliquid had an enhancing effect through the random motion variable. Fig. 13 depicts the concentration performance for the Schmidt number. An augmentation in concentration was seen through the Schmidt number. Fig. 14 depicts ($\phi(\zeta,\eta)$) against (Nt). A decreasing trend for concentration was seen through the thermophoresis variable variation.

6 Entropy rate

Fig. 15 illustrates the entropy performance considering the Brinkman (Br) number. Clearly, the entropy rate increased with the Brinkman number. The effect of the variation of the

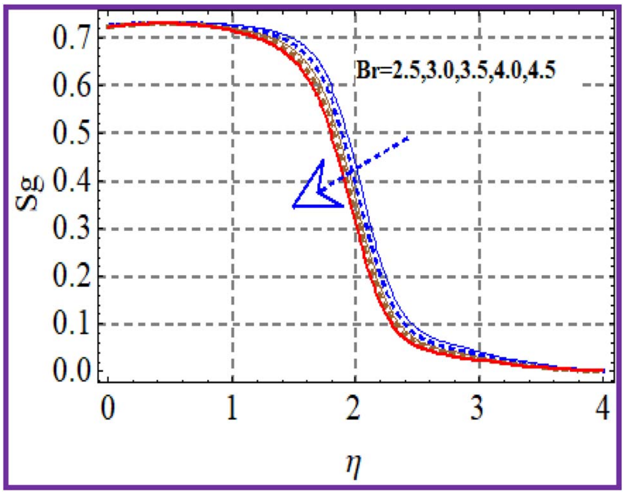

Fig. 15 S_g *via* Br.

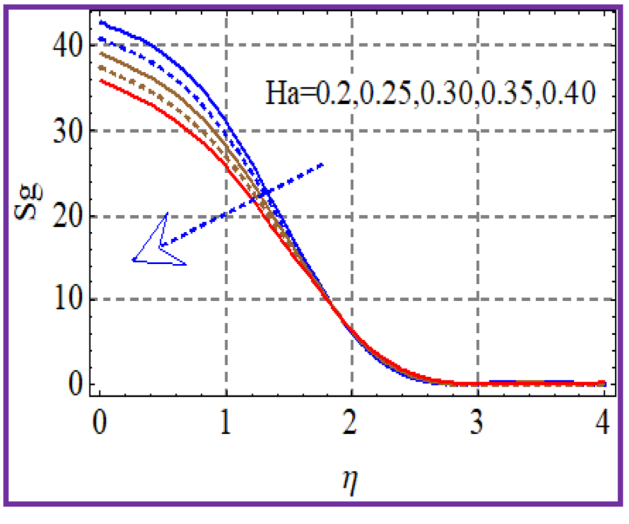

Fig. 16 S_g *via* Ha.

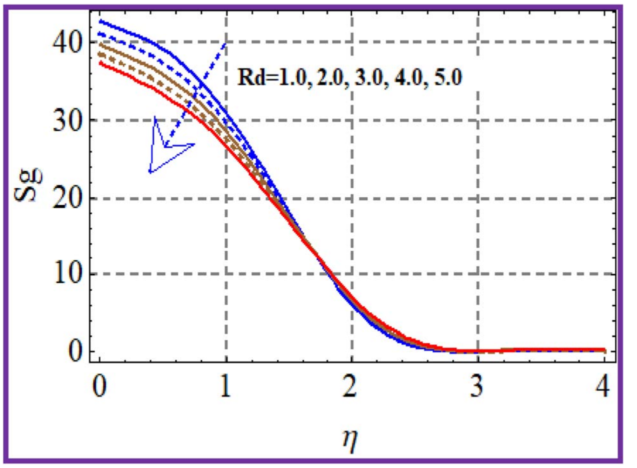

Fig. 17 S_g *via* Rd.

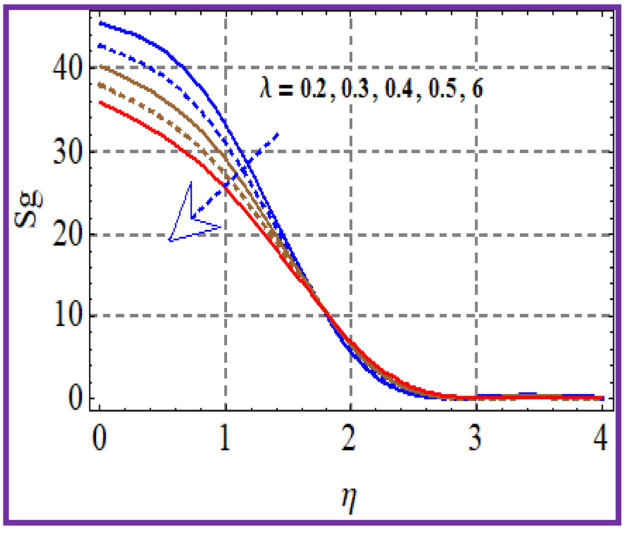

Fig. 18 S_g *via* λ.

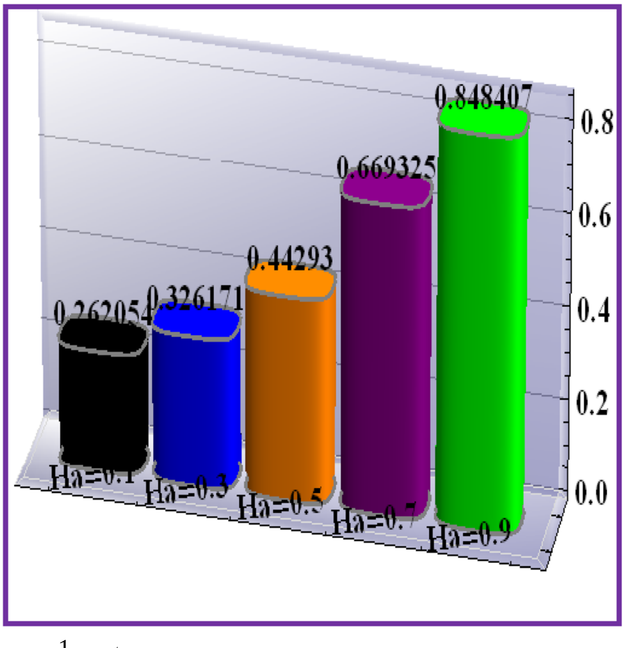

Fig. 19 $\frac{1}{2}\mathrm{Re}_x^{1/2}C_f$ *via* Ha.

© 2023 The Author(s). Published by the Royal Society of Chemistry

Open Access Article. Published on 15 November 2023. Downloaded on 7/29/2025 9:28:29 PM.
This article is licensed under a Creative Commons Attribution-NonCommercial 3.0 Unported Licence.

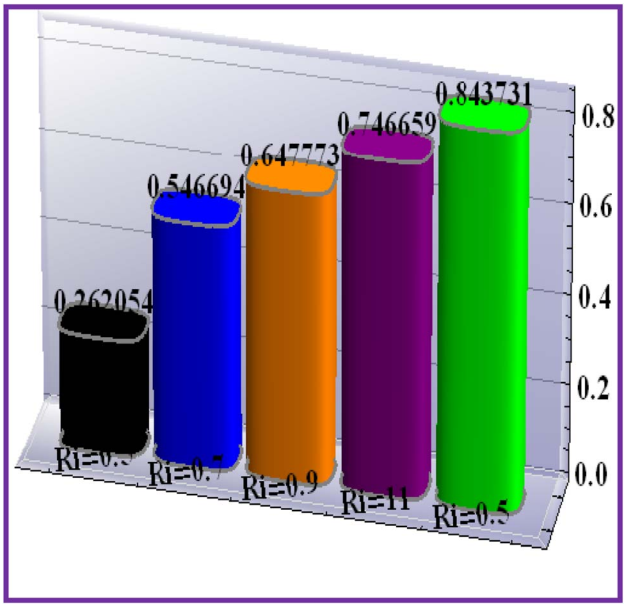

Fig. 20 $\frac{1}{2}\mathrm{Re}_x{}^{1/2}C_f$ *via* Ri.

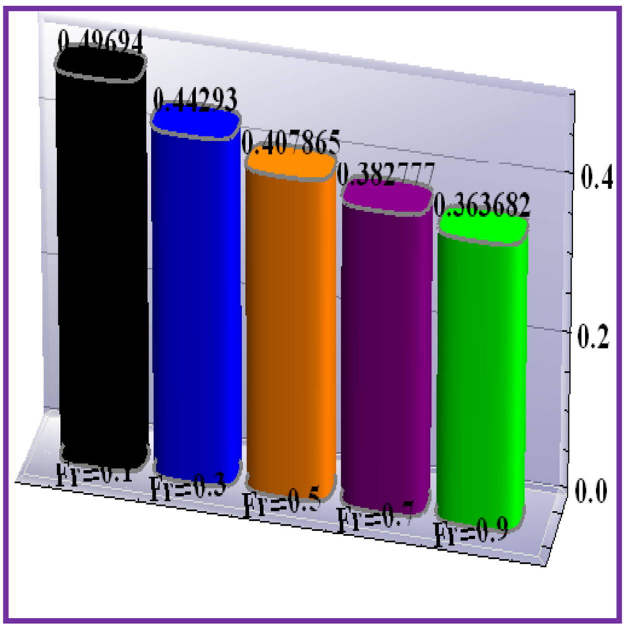

Fig. 21 $\frac{1}{2}\mathrm{Re}_x{}^{1/2}C_f$ *via* Fr.

Hartman (Ha) number on (S_g) is portrayed in Fig. 16. A higher estimation of Hartman number decreased the entropy rate. Fig. 17 shows the impact of (S_g) *via* radiation. A decrease in entropy was detected against the radiation variable. From Fig. 18, it could be noticed that the entropy reduced with higher porosity.

7 Quantities under interest

Graphical illustrations for the skin friction coefficient and Nusselt number are addressed.

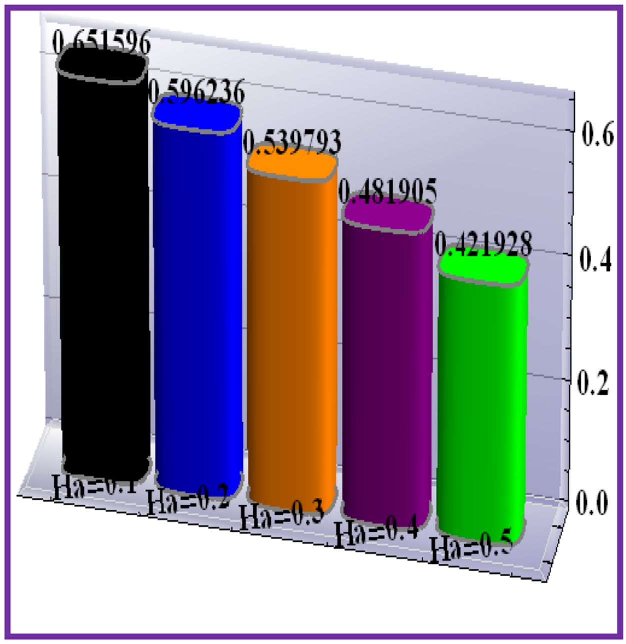

Fig. 22 $\mathrm{Re}^{1/2}\mathrm{Nu}$ *via* Ha.

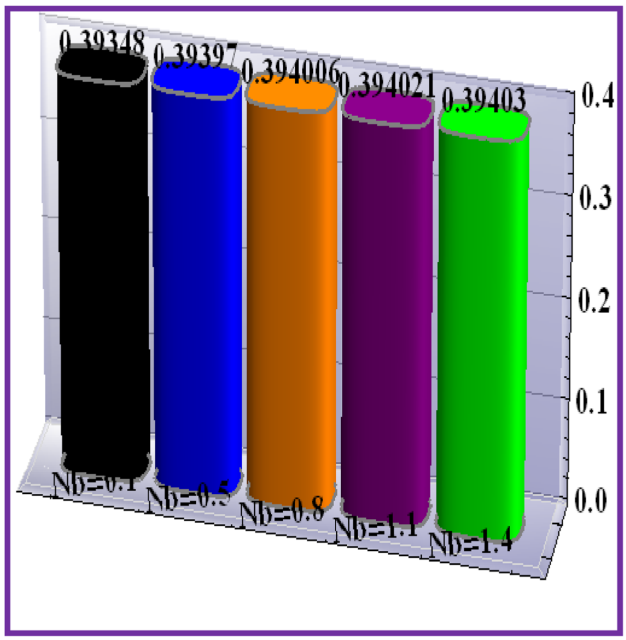

Fig. 23 $\mathrm{Re}^{1/2}\mathrm{Nu}$ *via* Nb.

7.1 Skin friction coefficient

Fig. 19–21 display the impacts of the velocity gradient with the Hartman number, mixed convection variable, and Forchheimer number. An increasing behavior was observed against rising values of (Ha) and (Ri), but the opposite scenario held for (Fr).

7.2 Heat transfer rate

The impact of emerging variables ((Nt), (Nb) and (Ec)) on ($\mathrm{Re}^{1/2}\mathrm{Nu}$) are displayed in Fig. 22–24. Clearly, the thermal transport

© 2023 The Author(s). Published by the Royal Society of Chemistry

Open Access Article. Published on 15 November 2023. Downloaded on 7/29/2025 9:28:29 PM.
This article is licensed under a Creative Commons Attribution-NonCommercial 3.0 Unported Licence.

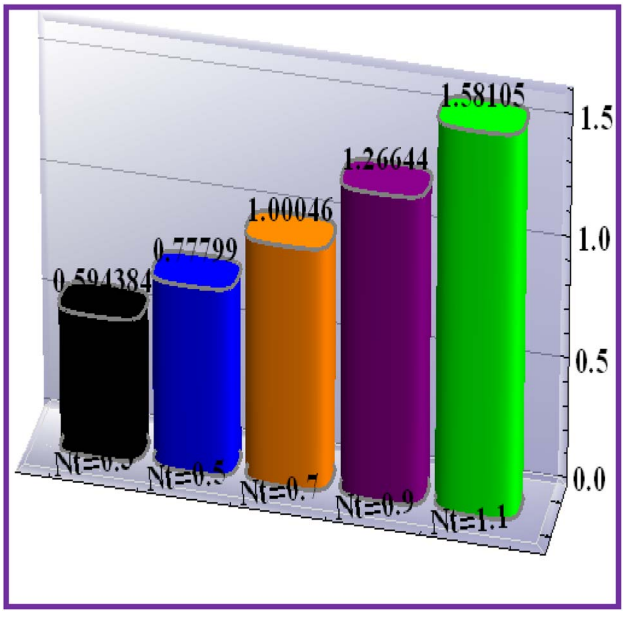

Fig. 24 $Re^{1/2}Nu$ *via* Nt.

rate increased *versus* higher random motion (Nb) and thermophoresis (Nb) variables. From Fig. 7b, it could be detected that the heat transport rate declined for higher Eckert numbers.

8 Conclusions

Key observation are listed below.

≫ Mixed convection and porosity had opposite impacts on the flow.

≫ Hartman number yielded an opposite outcome for the flow and entropy rate.

≫ Flow was decreased by Forchheimer number.

≫ An enhancement in Hartman number led to enhanced drag force and higher temperature.

≫ Higher Eckert numbers led to an enhancement in temperature.

≫ Prandtl number led to a reduction in temperature.

≫ An opposite trend for entropy and thermal field was witnessed through considering radiation.

≫ An enhancement in temperature and the heat transport rate were noticed for the thermophoresis variable.

≫ Concentration was reduced *versus* a higher thermophoresis variable.

≫ Increasing trend for concentration was noted through the Schmidt number.

≫ Brinkman number corresponded an enhancement in entropy.

≫ Thermal transport rate surged upwards against the random motion variable.

≫ Decrease in entropy rate was witnessed *versus* the Brinkman number.

≫ Higher Eckert numbers decreased the temperature gradient.

Further investigations in the future should consider bioconvection and motile microorganisms, of which almost nothing is known yet. Such attempts for mixed, bioconvection and Marangoni convection, activation energy and slip and melting conditions should be examined.

Abbreviations

u,v	Velocity components
k_r	Reaction rate
x,y	Cartesian coordinates
L	Reference length
Ω	Inclination angle
R	Molar gas constant
ν_f	Kinematic viscosity
ψ	Stream function
g	Gravity
Re_x	Local Reynolds number
β	Thermal expansion coefficient
Ha	Magnetic variable
ρ_f	Density
Gr	Grashoff number
σ_f	Electrical conductivity
Ri	Mixed convection variable
B_0	Magnetic field strength
Re	Reynolds number
ρ_p	Nanoparticle density
λ	Porosity variable
ρ_{f_∞}	Nanofluid density
Fr	Forchheimer number
$F=\left(\frac{C_b}{\sqrt{k_p}}\right)$	Inertia coefficient
Nt	Thermophoresis variable
C_b	Drag force coefficient
Pr	Prandtl number
k_p	Porous medium permeability
Rd	Radiation variable
T	Temperature
Nb	Brownian motion variable
T_w	Wall temperature
Ec	Eckert number
T_∞	Ambient temperature
k_1	Reaction variable
α_f	Thermal diffusivity
Br	Brinkman number
$\tau=\left(\frac{(\rho c_p)_p}{(\rho c_p)_f}\right)$	Ratio of heat capacitance
C_f	Skin friction coefficient
σ^*	Stefan–Boltzmann constant
τ_w	Wall shear stress
D_T	Thermophoresis coefficient
Nu	Nusselt number
k^*	Mean absorption coefficient
Sh	Sherwood number
D_B	Brownian diffusion coefficient
q_w	Heat flux
c_p	Specific heat

© 2023 The Author(s). Published by the Royal Society of Chemistry

Open Access Article. Published on 15 November 2023. Downloaded on 7/29/2025 9:28:29 PM.
This article is licensed under a Creative Commons Attribution-NonCommercial 3.0 Unported Licence.

J_w	Mass flux
C	Concentration
S_g	Entropy rate
C_w	Wall concentration
α_1	Temperature difference variable
C_∞	Ambient concentration
L_1	Diffusion variable
u_∞	Reference velocity
α_2	Concentration difference variable

Conflicts of interest

There are no conflicts to declare.

References

1 S. U. S. Choi, Enhancing thermal conductivity of fluids with nanoparticle, *ASME J. Fluids Eng. Publication Fed.*, 1995, **231**, 99–105.

2 J. Buongiorno, Convective transport in nanofluids, *ASME J. Heat Mass Transfer*, 2006, **128**, 240–250.

3 I. Waini, K. B. Hamzah, N. S. Khashiie, N. A. Zainal, A. R. M. Kasim, A. Ishak and I. Pop, Brownian and thermophoresis diffusion effects on magnetohydrodynamic Reiner–Philippoff nanofluid flow past a shrinking sheet, *Alexandria Eng. J.*, 2023, **67**, 183–192.

4 G. Kalpana, K. R. Madhura and R. B. Kudenatti, Numerical study on the combined effects of Brownian motion and thermophoresis on an unsteady magnetohydrodynamics nanofluid boundary layer flow, *Math. Comput. Simul.*, 2022, **200**, 78–96.

5 P. M. Patil and M. Kulkarni, MHD quadratic mixed convective Eyring-Powell nanofluid flow with multiple diffusions, *Chin. J. Phys.*, 2022, **77**, 393–410.

6 H. Upreti, A. K. Pandey, Z. Uddin and M. Kumar, Thermophoresis and Brownian motion effects on 3D flow of Casson nanofluid consisting microorganisms over a Riga plate using PSO: a numerical study, *Chin. J. Phy.*, 2022, **78**, 234–270.

7 S. A. Khan, T. Hayat and A. Alsaedi, Entropy generation in chemically reactive flow of Reiner-Rivlin liquid conveying tiny particles considering thermal radiation, *Alexandria Eng. J.*, 2023, **66**, 257–268.

8 B. Ali, P. K. Pattnaik, R. A. Naqvi, H. Waqas and S. Hussain, Brownian motion and thermophoresis effects on bioconvection of rotating Maxwell nanofluid over a Riga plate with Arrhenius activation energy and Cattaneo-Christov heat flux theory, *Therm. Sci. Eng. Prog.*, 2021, **23**, 100863.

9 M. Mustaq, S. Asghar and M. A. Hossian, Mixed convection flow of second grade fluid along vertical stretching flat surface with variable surface temperature, *Heat Mass Transfer*, 2007, **43**, 1049–1061.

10 T. Hayat, T. Muhammad, S. A. Shehzad, G. Q. Chen and I. A. Abbas, Interaction of magnetic field in flow of Maxwell nanofluid with convective effect, *J. Magn. Magn. Mater.*, 2015, **389**, 48–55.

11 F. Mabood, M. D. Shamshuddin and S. R. Mishra, Characteristics of thermophoresis and Brownian motion on radiative reactive micropolar fluid flow towards continuously moving flat plate: HAM solution, *Math. Comput. Simul.*, 2022, **191**, 187–202.

12 S. Ahmed, H. Xu, Y. Zhou and Q. Yu, modelling convective transport of hybrid nanofluid in a lid driven square cavity with consideration of Brownian diffusion and thermophoresis, *Int. Commun. Heat Mass Transfer*, 2022, **137**, 106226.

13 S. Patil, C. Kataria, A. Kumar and A. Kumar, Effect of segregation and advection governed heterogeneous distribution of nanoparticles on NEPCM discharging behavior, *Journal of Energy Storage*, 2023, **57**, 106230.

14 G. Rasool, N. A. Ahammad, M. R. Ali, N. A. Shah, X. Wang, A. Shafiq and A. Wakif, Hydrothermal and mass aspects of MHD non-Darcian convective flows of radiating thixotropic nanofluids nearby a horizontal stretchable surface: passive control strategy, *Case Stud. Therm. Eng.*, 2023, **42**, 102654.

15 M. Turkyilmazoglu, Nanofluid flow and heat transfer due to a rotating disk, *Comput. Fluids*, 2014, **94**, 139–146.

16 A. Majeed, N. Golsanami, B. Gong, Q. A. Ahmad, S. Rifaqat, A. Zeeshan and F. M. Noori, Analysis of thermal radiation in magnetohydrodynamic motile gyrotactic micro-organisms flow comprising tiny nanoparticle towards a nonlinear surface with velocity slip, *Alexandria Eng. J.*, 2023, **66**, 543–553.

17 M. Yasir, A. Ahmed, M. Khan, A. K. Alzahrani, Z. U. Malik and A. M. Alshehri, Mathematical modelling of unsteady Oldroyd-B fluid flow due to stretchable cylindrical surface with energy transport, *Ain Shams Eng. J.*, 2023, **14**, DOI: 10.1016/j.asej.2022.101825.

18 M. Basavarajappa and D. Bhatta, Unsteady nonlinear convective flow of a nanofluid over a vertical plate due to impulsive motion: optimization and sensitivity analysis, *Int. Comm. Heat Mass Transf.*, 2022, **134**, 106036.

19 M. Hussain and M. Sheremet, Convection analysis of the radiative nanofluid flow through porous media over a stretching surface with inclined magnetic field, *Int. Commun. Heat Mass Transfer*, 2023, **140**, 106559.

20 H. Khoshtarash, M. Siavashi, M. Ramezanpour and M. J. Blunt, Pore-scale analysis of two-phase nanofluid flow and heat transfer in open-cell metal foams considering Brownian motion, *Appl. Therm. Eng.*, 2023, **221**, 119847.

21 A. Bejan, A study of entropy generation in fundamental convective heat transfer, *J. Heat Transfer*, 1979, **101**, 718–725.

22 A. Bejan, Second law analysis in heat transfer, *Energy*, 1980, **5**, 721–732.

23 A. Dawar, Z. Shah, W. Khan, M. Idrees and S. Islam, Unsteady squeezing flow of magnetohydrodynamic carbon nanotube nanofluid in rotating channels with entropy generation and viscous dissipation, *Adv. Mech. Eng.*, 2019, **11**, 1–18.

24 T. Hayat, L. Sajjad, M. I. Khan, M. I. Khan and A. Alsaedi, Salient aspects of thermodiffusion and diffusion thermo

Open Access Article. Published on 15 November 2023. Downloaded on 7/29/2025 9:28:29 PM.
This article is licensed under a Creative Commons Attribution-NonCommercial 3.0 Unported Licence.

on unsteady dissipative flow with entropy generation, *J. Mol. Liq.*, 2019, **282**, 557–565.
25 K. B. Sharma, R. Gandhi and M. M. Bhatti, Entropy analysis of thermally radiating MHD slip flow of hybrid nanoparticles (Au-Al2O3/Blood) through a tapered multi-stenosed artery, *Chem. Phys. Lett.*, 2022, **790**, 139348.
26 S. A. Khan, T. Hayat and A. Alsaedi, Entropy optimization for nanofluid flow with radiation subject to a porous medium, *J. Pet. Sci. Eng.*, 2022, **217**, 110864.
27 B. Iftikhar, T. Javed and M. A. Siddiqu, Entropy generation analysis during MHD mixed convection flow of non-Newtonian fluid saturated inside the square cavity, *J. Comput. Sci.*, 2023, **66**, 101907.
28 T. Hayat, A. Razaq, S. A. Khan and S. Momani, Soret and Dufour impacts in entropy optimized mixed convective flow, *Int. Commun. Heat Mass Transfer*, 2023, **141**, 106575.
29 H. Maiti, A. Y. Khan, S. Mondal and S. K. Nandy, Scrutinization of unsteady MHD fluid flow and entropy generation: Hybrid nanofluid model, *J. Comput. Appl.*, 2023, **6**, 100074.
30 M. Sankar, H. A. K. Swamy, Q. A. Mdallal and A. Wakif, Non-Darcy nanoliquid buoyant flow and entropy generation analysis in an inclined porous annulus: effect of source-sink arrangement, *Alexandria Eng. J.*, 2023, **68**, 239–261.
31 M. M. Bhatti and S. I. Abdelsalam, Scientific breakdown of a ferromagnetic nanofluid in hemodynamics: enhanced therapeutic approach, *Math. Modell. Nat. Phenom.*, 2022, **17**, DOI: 10.1051/mmnp/2022045.
32 M. M. Bhatti and R. Ellahi, Numerical investigation of non-Darcian nanofluid flow across a stretchy elastic medium with velocity and thermal slips, *Numer. Heat Transfer, Part B*, 2023, **83**, 323–343.
33 N. Vedavathi, G. Dharmaiah, S. A. Gaffar and K. Venkatadri, Entropy analysis of nanofluid magnetohydrodynamic convection flow past an inclined surface: a numerical review, *Heat Transfer*, 2021, **50**(6), 5996–6021.
34 E. M. Sparrow and H. S. Yu, Local non-similarity thermal boundary-layer solutions, *J. Heat Transfer*, 1971, **93**, 328–334.
35 R. Razzaq, U. Farooq, J. Cui and T. Muhammad, Non-similar solution for magnetized flow of Maxwell nanofluid over an exponentially stretching surface, *Math. Probl. Eng.*, 2021, **2021**, DOI: 10.1155/2021/5539542.
36 C. Y. Wang, Free convection on a vertical stretching surface, *J. Appl. Math. Mech.*, 1989, **69**, 418–420.

 © 2023 The Author(s). Published by the Royal Society of Chemistry